Solar Energy Materials & Solar Cells 114 (2013) 24–30

Contents lists available at SciVerse ScienceDirect

Solar Energy Materials & Solar Cells

journal homepage: www.elsevier.com/locate/solmat

Facile hot solvent vapor annealing for high performance polymer solar cell using spray process

Yu-Ching Huang [a,*], Hou-Chin Chia [a], Chih-Min Chuang [a], Cheng-Si Tsao [a], Charn-Ying Chen [a], Wei-Fang Su [b,**]

[a] Institute of Nuclear Energy Research, Longtan, Taoyuan 325-46, Taiwan
[b] Department of Materials Science and Engineering, National Taiwan University, Taipei 106-17, Taiwan

ARTICLE INFO

Article history:
Received 28 November 2012
Received in revised form
9 February 2013
Accepted 20 February 2013

Keywords:
Charge transport
Nanostructures
Organic electronics
Solar cells
Spray process

ABSTRACT

In this paper, the use of hot solvent vapor (HSV) annealing is demonstrated to improve the performance of polymer solar cells (PSCs) fabricated by the spray process. The blend of poly(3-hexylthiophene) and [6,6]-phenyl-C_{61}-butyric acid methyl ester (P3HT/PCBM) is used as a photoactive layer of the solar cell. Compared to the conventional solvent vapor annealing, the HSV annealing can eliminate the formation of intra-droplet boundary during the spray process and optimize the nanostructure of the film quickly ($\leq$5 min). The study of conducting atomic force microscopy (C-AFM) reveals that the HSV annealed film exhibits smooth film surface and homogenous conductivity distribution. Moreover, an enhanced light harvesting and increased crystallinity of P3HT in the active layer are observed by UV–vis absorption and X-ray diffraction (XRD). With subsequent thermal annealing, the power conversion efficiency of solar cell made from the HSV annealed film is reached at 3.61%. This HSV annealing technique can be implemented into the fabrication of high efficient large-area PSCs using the spray process.

1. Introduction

Polymer solar cell (PSC) has potential to become next generation of low cost and flexible solar cell due to its ease of processing from solution into large area [1–4]. Due to relatively low power conversion efficiency (PCE) of PSC fabricated from P3HT/PCBM, the enhancement of PCE has been obtained by design and synthesis of new conjugated polymer [5–7] and fullerene derivatives [8–10]. A PCE of about 9% was achieved recently [11]. Furthermore, the morphology of active layers is critical to the overall PCE improvement of PSCs. A bi-continuous network of bulk heterojunctions (BHJs) is formed in the active layer, so an efficient charge transport can occur [12–15]. Due to the small exciton diffusion length (on the order of ~10 nm) [16,17], the nanoscale morphology of BHJs is important to the solar cells performance [18–22]. Several approaches have been proposed to manipulate the phase-separated nanostructures, including thermal annealing [23–25], solvent mixture [26,27], slow growth [28,29] and solvent vapor annealing [30–32]. Therein, thermal annealing is the most effective approach to enhance the PCE of solar cells. However, most of the previous studies have focused on the optimization of nanostructured thin films ($\leq$250 nm) processed by the spin-coating technique, which is not suitable for mass production. To facilitate the mass production, in-line compatible deposition methods have been developed [33–39]. The spray process has been emerged as a low cost fabricating process for large-area devices because of its high throughput rate and low material waste. However, it is difficult to control the film thickness below 250 nm with desired morphology using the spray process.

In addition, the PCE of the PSC fabricated by the spray process is also limited by the series resistance (R_s) resulting from the presence of inter-droplet boundary in sprayed films. The problem has been reduced with improved PCE by using co-solvent [35,40], multi-source deposit [41] and spraying solvent over layer [42]. These results were obtained by optimizing the film drying kinetics, i.e. controlling the film drying time within 10 min. If we could further control the film drying kinetics, we would achieve higher enhancement in PCE.

In this paper, we demonstrated a facile method, hot solvent vapor (HSV) annealing, to control the sprayed film morphology. Traditional solvent vapor annealing takes about 1 h to accomplish. Conversely, the HSV annealing takes only a few minutes to eliminate the inter-droplet boundary and reduce the R_s because the hot solvent vapor can effectively penetrate the films. Moreover, the surface morphology and the internal structure of the films can be

* Corresponding author. Tel.: +886 3 4711409x6426.
** Corresponding author. Tel.: +886 2 33664078.
E-mail addresses: huangyc@iner.gov.tw (Y.-C. Huang), suwf@ntu.edu.tw (W.-F. Su).

0927-0248/$ - see front matter © 2013 Elsevier B.V. All rights reserved.
http://dx.doi.org/10.1016/j.solmat.2013.02.022

uniformly re-constructed by HSV annealing. After the HSV annealing, a ~20% improvement in PCE was achieved (2.12%) as compared to that of the as-sprayed film. Furthermore, the PCE of HSV annealed device with subsequent thermal annealing was further increased to 3.61%. Our study could pave a way to the fabrication of high efficient spray solar cells using the spray process.

2. Experimental

2.1. Materials

P3HT and PCBM are supplied from Rieke Metals. Inc. PEDOT:PSS is supplied from Baytron company. All the solvents used in this study are supplied from Aldrich company.

2.2. Active layer deposited by spray process

The P3HT/PCBM solution was first prepared by dissolving 2 mg of P3HT and 2 mg of PCBM in 1 ml of chlorobenzene (CB), stirred overnight at 45 °C in a glove box. Prior to the film fabrication, the ITO glass substrate was ultrasonically cleaned in a series of organic solvents (methanol, acetone, and isopropanol) and then treated with UV/ozone for 10 min. Poly(3,4-ethylenedioxythiophene) doped with polystyrene sulfonic acid, PEDOT:PSS (Baytron AI 4083), was used as a hole transport layer (HTL). A 40-nm-thick layer of PEDOT:PSS was deposited on a cleaned ITO glass substrate by spin-coating at 5000 rpm for 1 min and drying at 120 °C for 20 min. The active layer was spray-coated in ambient conditions using an ExactaCoat system equipped with an AccuMist 120 kHz ultrasonic atomizing nozzle (Sono-Tek Corporation). Fig. 1 shows the schematic diagram of this system which is constructed by combining an ultrasonic atomizing nozzle with a controlled jet of air from the flat jet air deflector. An auto-solution injection controller (Fig. 1a) controls the injected flow rate of P3HT/PCBM solution into the ultrasonic nozzle from a solution inlet (Fig. 1c). The ultrasonic nozzle as shown in Fig. 1e can atomize P3HT/PCBM solution into droplets of about 15 μm in size. To spray the droplets of P3HT/PCBM onto the PEDOT:PSS coated ITO substrate, an air stream is flowed into flat jet air deflector (Fig. 1d) from an air inlet (Fig. 1b). The air stream allows low or high-impact of the atomized droplets onto the substrate by tuning the pressure of air stream from the air deflector. In our study, the injected flow rate of P3HT/PCBM solution was 0.1 ml min^{-1} and the pressure of air stream was ~0.6 MPa. The ultrasonic nozzle tip was kept at 10 cm distance from the substrate. In this spray condition, the thickness of P3HT/PCBM films was ca. 300 nm.

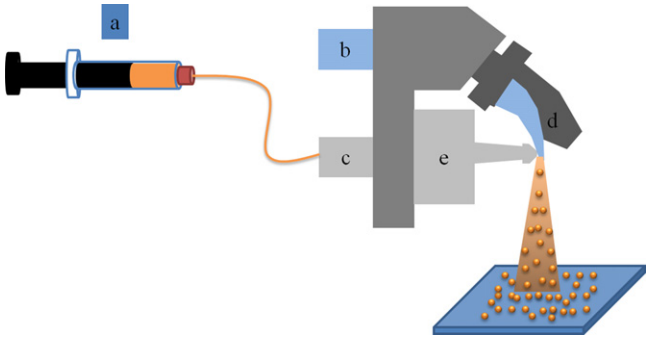

Fig. 1. Schematic diagram of spray-coater. (a) Auto-solution injection controller: control the injected flow rate of P3HT/PCBM blend solution; (b) air inlet: allow air stream to flow into air deflector; (c) solution inlet: allow P3HT/PCBM blend solution to be injected into ultrasonic nozzle; (d) flat jet air deflector: control air stream pressure to allow low or high-impact of the atomized spray onto the substrate; and (e) ultrasonic nozzle: atomized P3HT/PCBM blend solution into droplet.

2.3. Annealing treatment

For HSV annealing, 1,2-dichlorobenzene (DCB) was heated at various temperatures (45 °C~75 °C) in a Petri dish. P3HT/PCBM films were put into the Petri dish filled with hot DCB vapor for a few minutes and the surface of films would gradually become wet. After HSV annealing, the films were left to dry for roughly 1 min in ambient. For thermal annealing, the films were thermally annealed at 130 °C for 10 min in a glove box before cathode deposition.

2.4. Active layer characterization

The formation of intra-droplet boundary during the spray process was studied by an optical microscope (OM, Leica Microsystems, DM1750M). The morphology and conductivity of films were characterized using conducting atomic force microscope (C-AFM, Veeco, CP-II). A Pt/Ir_5 coated tip used in C-AFM setup serves as a mobile electrode to record morphology and local electric property simultaneously. UV–vis absorption spectroscopy (PerkinElmer Lambda 35) was used to monitor the absorption spectra of films. The thickness and surface profile of films were measured using a stylus profiler (AlphaStep D-100, KLA Tencor). A high resolution X-ray diffractometer (Rigaku TTRXA 3) was used to study the crystallinity of P3HT.

2.5. Device fabrication and characterization

After annealing treatment, the films were deposited with Ca and Al as cathode using thermal evaporation. ~30 nm of Ca and ~100 nm of Al were sequentially deposited at a high vacuum of 5×10^{-6} torr. The device area was determined by the covered cathode area because we did not etch the anode of ITO. In our study, the area of solar cells was 0.30 cm^2. The *J–V* characterization was evaluated under A.M. 1.5 illumination (100 mW/cm^2) using a solar simulator (Abet technologies, Model # 11000). The EQE spectra were recorded under the illumination of a xenon lamp and a monochromator (Enlitech, QE-R).

3. Results and discussion

All the films of active layer of solar cells were prepared by the spray process; we called them as-sprayed films. The names of as-sprayed films after different treatments are defined as following: TA means thermal annealed film; the HSV annealed films were labeled according to the solvent vapor temperature and annealing time. For instance, the 45 °C 2 min HSV annealed film means the as-sprayed film was treated by the HSV at 45 °C for 2 min.

3.1. Morphology evolution and local electric property of HSV annealed films

The morphology of HSV annealed films at different conditions was studied by optical microscopy as shown in Fig. 2. Fig. 2a shows the as-sprayed P3HT/PCBM film which exhibits a heterogeneous morphology. An obvious droplet boundary was observed in the film which would generate a barrier to slow charge transport. The amount of droplet boundary was decreased sharply after solvent vapor annealing at 45 °C for 2 min, but there were few droplet boundaries remained (Fig. 2b). The droplet boundaries were further reduced by increasing the annealing time to 4 min (Fig. 2c). When the solvent vapor temperature was increased to 55 °C, the droplet boundary was eliminated regardless of 2 min (Fig. 2d) or 4 min (Fig. 2e) annealing time. Previous studies [38,39] have pointed out

that the elimination of droplet boundary and continuous network contributed a reduction in R_s.

We employed the conducting atomic force microscopy (C-AFM) to study the morphology and local electric property simultaneously. The topographic and electronic images of as-sprayed film and HSV annealed film at 55 °C for 4 min (55 °C 4 min) are shown in Fig. 3. The RMS roughness of the as-sprayed film was dramatically reduced from 114.5 nm to 3.7 nm after this annealing. A significant reduction in the film roughness suggests that active layer contained fewer voids. Thus, the film could provide a good contact with cathode and result in increased shunt resistance (R_{sh}) [43]. Moreover, the HSV annealed film showed improved film continuity. The enhanced interfacial contact and improved film continuity also facilitate effective charge transport.

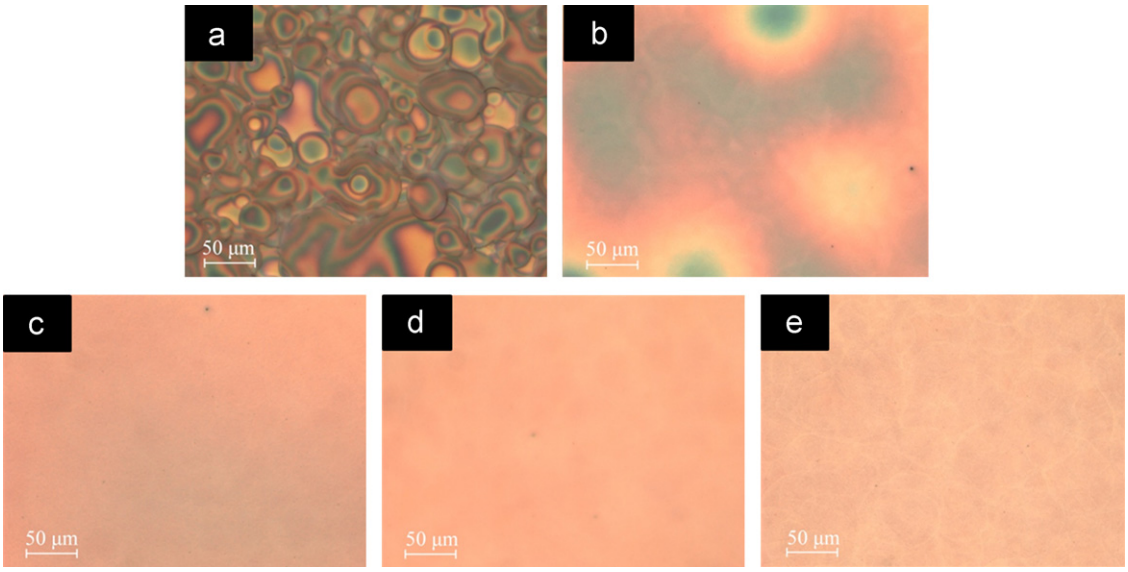

Fig. 2. Optical images of sprayed film with various HSV annealing. (a) As-sprayed film, (b) HSV annealed film at 45 °C for 2 min, (c) HSV annealed film at 45 °C for 4 min, (d) annealed film at 55 °C for 2 min, and (e) HSV annealed film at 55 °C for 4 min.

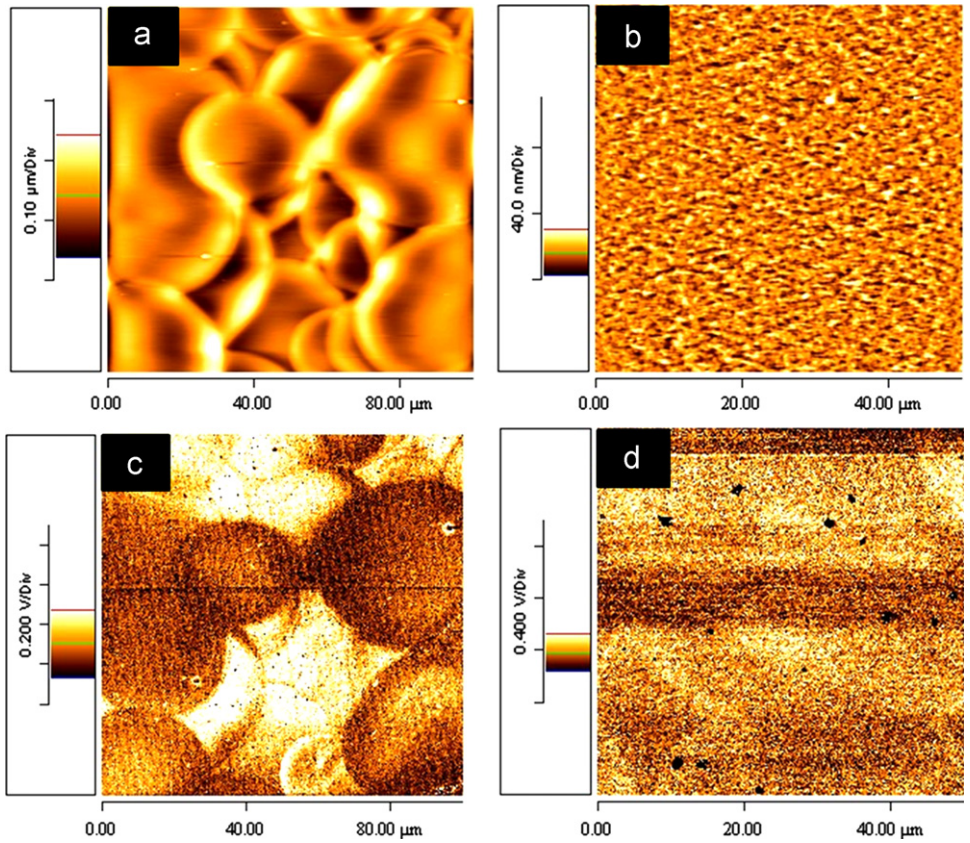

Fig. 3. Topographic AFM images of (a) as-sprayed film and (b) HSV annealed film at 55 °C for 4 minutes. Conducting AFM images of (c) as-sprayed film and (d) HSV annealed film at 55 °C for 4 min.

The results of conducting AFM further support the speculation of facile charge transport. The electronic image of the as-sprayed film (Fig. 3c) clearly indicates a heterogeneous charge distribution resulting from the hindered charge transport at the conducting boundary of the film. Whereas, the HSV annealed film shows a homogeneous conductivity distribution without charge transport barriers as shown in Fig. 3d. This result provides us insights into the role of HSV annealing in the formation of nanoscale morphology and improved conductivity.

3.2. Absorption and crystallinity characterization of HSV annealed films

The absorption spectra of P3HT/PCBM films under different HSV treatments are shown in Fig. 4. We observe an increasing absorbance of films after various HSV annealing. This implies that the $\pi-\pi$ stacking of the P3HT molecules is enhanced with high chain ordering [44]. Also, a development of the vibronic shoulders near 610 nm wavelength corresponds to the enhanced inter-chain P3HT stacking ordering [45]. It is noteworthy that the PCBM absorption peak (~350 nm) increases with the HSV annealing. Our previous research [44] indicated that the absorption peak of PCBM did not change under thermal annealing at 140 °C for 30 min. In addition, it was reported that the PCBM absorption peak was not increased with various external treatment [42]. This result implies that the HSV annealing not only increases the P3HT chain stacking ordering but also induces PCBM cluster formation. An appropriate PCBM clustering process was reported to enhance the OPV performance due to the formation of good pathway for charge transport [46]. In other words, the HSV annealing process provides an alternative way to control the formation of PCBM cluster when the active layer of solar cell was fabricated using the spray process. Fig. 4b shows the absorption spectra of the different films with subsequent thermal annealing at 130 °C for 10 min. The absorbance and vibronic shoulder could be further increased with subsequent thermal treatment. It signifies that the chain stacking of P3HT is considerably improved after the HSV with subsequent thermal treatment. The results of absorption study are consistent with the results of XRD study (Fig. 5). The characteristic (100) peak (2θ ~5.4°) mainly comes from the oriented edge-on P3HT crystallites with lamellar structure (stacking by polymer backbones) parallel to the substrate. The enhanced crystallinity of P3HT is observed from increased intensity of (100) peak upon increasing HSV temperature or annealing time. Notably, the HSV annealed film at 55 °C for 4 min (55 °C 4 min) shows a decreasing intensity of (100) peak as compared to that of the HSV annealed film at 55 °C for 2 min (55 °C 2 min). This result implies that the P3HT/PCBM film tends to lose its crystallinity at 55 °C for an extended period of time. We inferred that a conformation chain defect of P3HT is occurred because the PCBM molecules might interrupt the ordering of P3HT chain stacking with an extended HSV time at 55 °C. Furthermore, the intensity of the (100) peak was further enhanced by subsequent thermal annealing for a better thermodynamic equilibrium of crystallization. This result is consonant with what we conclude from the analysis of absorption spectra.

3.3. HSV annealed solar cell characterization and external quantum efficiency measurement

Fig. 6 is a simplified cross-section schematic diagram showing the effect of HSV annealing on the morphology and interfacial contact in P3HT/PCBM sprayed film. As-sprayed P3HT/PCBM film shown in Fig. 6a illustrates a poor interfacial contact between active layer and cathode due to the P3HT/PCBM droplets deposition. In addition, the stack of P3HT molecules and the formation of PCBM clusters are interrupted by the boundary of droplet. HSV annealed film shown in Fig. 6b presents the BHJ nanostructure features an appropriate degree of phase separation, which results in effective charge transport and film conductivity. Moreover, the good interfacial contact shown in Fig. 6b improves the charge collection at the cathode.

The current–voltage characteristics of devices fabricated from active layer with various treatments under A.M. 1.5 illumination are plotted in Fig. 7 and the overall photovoltaic performance of

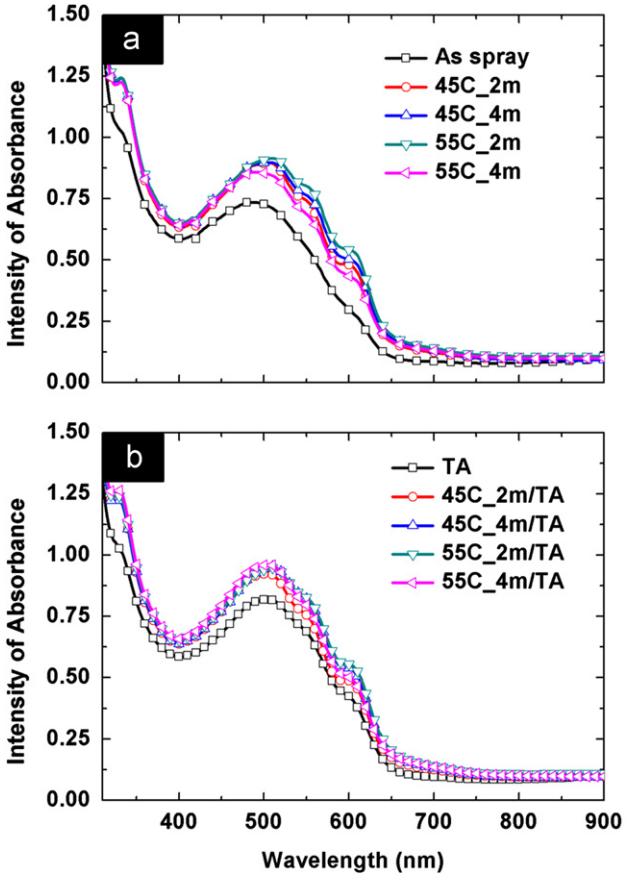

Fig. 4. Absorption spectra of sprayed film with various annealing treatments. (a) Films treated with various HSV annealing and (b) combining HSV annealing and the thermal annealing process.

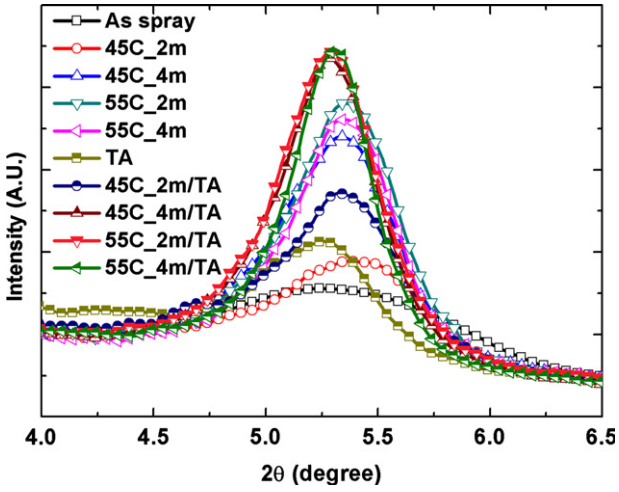

Fig. 5. Out-of-plane X-ray diffraction profiles of sprayed film with various annealing treatments.

these devices are represented in Table 1. A relative low PCE (1.73%) is observed for device with only thermal anneal (curve TA of Fig. 7) because of the low fill factor (FF) resulting from the insufficient elimination of inter-droplet boundary (high R_s and low R_{sh}). About 20% increase in PCE is achieved for the HSV annealed device at 45 °C for 2 min (45 °C_2 min), which can be explained by the increasing FF resulting from effective increase in R_{sh}. The increased R_{sh} from 194 to 317 Ωcm^2 indicates that the HSV annealing reduces charge recombination and current leakage due to the improved interfacial contact between active layer and cathode. This result confirms our observation from C-AFM morphology analysis. Moreover, a further enhancement in PCE was achieved by HSV annealed devices with subsequent thermal annealing. The PCE of the HSV annealed device at 45 °C for 2 min with thermal annealing (45 °C 2 min/TA) was reached at 2.67% with an open circuit voltage (V_{oc}) of 0.63 V, a short circuit current (J_{sc}) of 6.66 mA/cm^2, and a FF of 63.62%. Motivated by the efficient PCE enhancement, further PCE optimization of HSV annealed devices was attempted by combining subsequent thermal annealing. The PCE of the HSV annealed devices at 45 °C for 4 min with thermal annealing 45 °C was 3.03%, and the PCE of the HSV annealed devices at 55 °C for 2 min with thermal annealing (55 °C 2 min/TA) was achieved at 3.61% with a V_{oc} of 0.64, J_{sc} of 8.79 mA/cm^2, and FF of 64.13%. According to our previous results, the significantly improved J_{sc} could be attributed to the following: (1) the enhanced light harvesting, (2) the improved crystallinity of P3HT and (3) the effective charge transport from the reduced R_s and the increased R_{sh}. However, the PCE of HSV annealed devices at 55 °C for 4 min with thermal annealing (55 °C 4 min/TA) lowered to 3.20% with a V_{oc} of 0.63, J_{sc} of 8.19 mA/cm^2, and FF of 61.94%. This implies that the decrease in J_{sc} is a consequence of a reducing light harvesting and crystallinity of P3HT. Furthermore, the HSV annealed devices at 55 °C for 4 min with thermal annealing shows an increasing R_s in active layer. The amount of defects is also increased due to the decreasing in R_{sh}. These results are consonant with the XRD study. In addition, the decreased R_{sh} presented in this device also indicated the impaired interfacial contact because of the changed morphology of active layer at nano-scale [43]. The corresponding external quantum efficiency (EQE) spectra of various devices with different HSV annealing plus thermal annealing are shown in Fig. 8. All devices show similar EQE spectra which reveal the efficiency of exciton generation and J_{sc} conversion. The EQE of HSV annealed devices at 55 °C for 2 min with subsequent thermal annealing is the highest, which is a strong evidence for the high J_{sc} of this device.

Interestingly, the effect of "over-HSV-anneal" on reduced PCE was presented as the device treated with high temperature (55 °C) for a longer time (4 min). To clarify this effect, we further treated the devices with higher temperature or longer time to

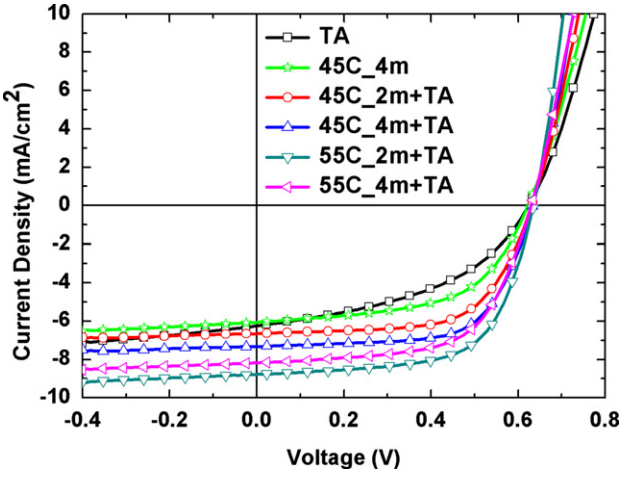

Fig. 7. *J–V* characteristics of PSCs with sprayed active layer under various annealing treatments.

Table 1
Performance of PSCs with sprayed active layer under various annealing treatment.

Treatment	V_{oc} (V)	J_{sc} (mA/cm^2)	FF (%)	PCE (%)	R_s (Ωcm^2)	R_{sh} (Ωcm^2)
TA	0.62	6.271	44.41	1.73	12.85	194.17
45 °C 2 min	0.62	6.068	56.31	2.12	12.27	317.46
45 °C 2 min/TA	0.63	6.66	63.62	2.67	8.86	909.09
45 °C 4 min/TA	0.63	7.33	65.51	3.03	7.54	917.43
55 °C 2 min/TA	0.64	8.79	64.13	3.61	4.66	990.02
55 °C 4 min/TA	0.63	8.19	61.94	3.20	8.40	787.40

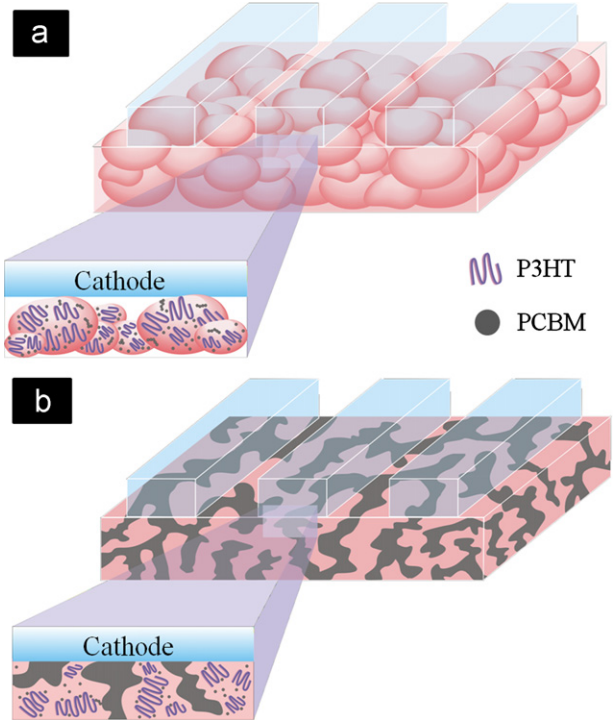

Fig. 6. Morphology of P3HT:PCBM sprayed films and interface conditions for P3HT:PCBM/cathode. (a) As-sprayed film and (b) HSV annealed film.

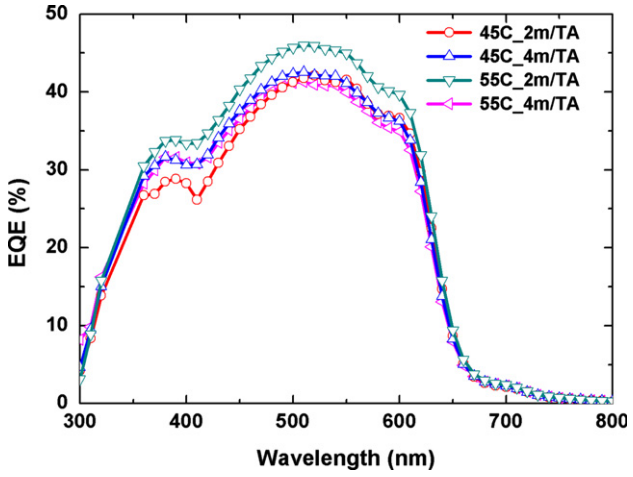

Fig. 8. External quantum efficiency (EQE) spectra of PSCs with sprayed active layer under various annealing treatments.

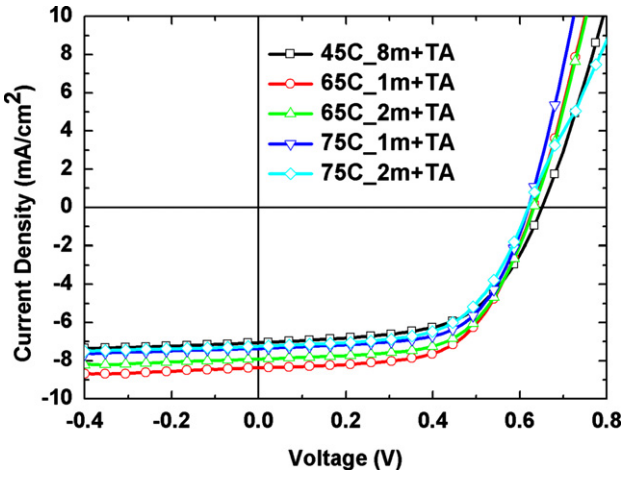

Fig. 9. *J–V* characteristics of various HSV annealed PSCs with subsequent thermal annealing.

Table 2
Performance of various HSV annealed PSCs with subsequent thermal annealing.

Treatment	V_{oc} (V)	J_{sc} (mA/cm^2)	FF (%)	PCE (%)
45 °C 8 min/TA	0.65	7.31	59.32	2.82
65 °C 1 min/TA	0.63	8.37	60.61	3.20
65 °C 2 min/TA	0.63	7.91	61.13	3.05
75 °C 1 min/TA	0.62	7.36	62.53	2.85
75 °C 2 min/TA	0.62	7.22	61.31	2.74

observe how the PCE was affected by the HSV anneal condition. The *J–V* curves were shown in Fig. 9 and the performances were listed in Table 2. A slight reduction in the PCE was observed in the HSV anneal device at 45 °C for 8 min with thermal anneal (45 °C 8 min/TA, 2.82%) as compared to the PCE of HSV anneal device at 45 °C for 4 min with thermal anneal (45 °C 4 min/TA, 3.03%). This result is consistent with what we observed in the HSV anneal device at 55 °C for an extended period of time, and it implies that the over-HSV-anneal would happen at a longer HSV anneal time and thus lower the PCE. We further raised the HSV anneal temperature to 65 °C and 75 °C and shortened the HSV anneal time to 1 and 2 min. The reduction of PCE from 3.20% (65C_1 m/TA) to 3.05% (65 °C 2 min/TA) indicates the devices suffer from the over-HSV-anneal in a shorter HSV anneal time at higher HSV anneal temperature as compared to that at lower HSV anneal temperature. Moreover, the PCE reduces further when the HSV anneal temperature raised up to 75 °C (2.85% and 2.74% for 75 °C 1 min/TA and 75 °C 2 min/TA, respectively). These implies that the PCE is strongly dependent on the HSV anneal condition, including anneal temperature and time.

4. Conclusions

We effectively improve the performance of P3HT/PCBM solar cells fabricated by the spray process through HSV annealing step. The HSV is a quick technique to control the morphology of the films and thus to enhance the PCE of the devices. Our study provides an alternative way to optimize the morphology of P3HT/PCBM sprayed films, including ordered P3HT chain stacking and PCBM cluster growing. As a result of this facile morphology controlling, about 20% increase in PCE is obtained in HSV annealed devices as compared to thermal annealed devices. Further optimal performance was reached by combining subsequent thermal annealing with HSV. The high PCE of 3.61% was achieved by sequential HSV annealing at 55 °C for 2 min plus thermal annealing. Therefore, we conclude that the HSV annealing technique presented in this study paves an important pathway to achieve high efficient large-area PSCs using the spray process.

Acknowledgment

We would like to thank Hsiu-Ming Chang, Yu-Chieh Tu, Wan-Yun Ho, Chia-Hsin Lee and Fan-Hsuan Hsu for helpful discussion.

References

[1] G. Dennler, M.C. Scharber, C.J. Brabec, Polymer–fullerene bulk-heterojunction solar cells, Advanced Materials 21 (2009) 1323–1338.
[2] T.D. Nielsen, C. Cruickshank, S. Foged, J. Thorsen, F.C. Krebs, Business, market and intellectual property analysis of polymer solar cells, Solar Energy Materials and Solar Cells 94 (2010) 1553–1571.
[3] S.W. Heo, K.W. Song, M.H. Choi, T.H. Sung, D.K. Moon, Patternable solution process for fabrication of flexible polymer solar cells using PDMS, Solae Energy Materials and Solar Cells 95 (2011) 3564–3572.
[4] S.Y. Park, Y.J. Kang, S. Lee, D.G. Kim, J.K. Kim, J.H. Kim, J.W. Kang, Spray-coated organic solar cells with large-area of 12.25 cm^2, Solar Energy Materials and Solar Cells 95 (2011) 852–855.
[5] J. Peet, J.Y. Kim, N.E. Coates, W.L. Ma, D. Moses, A.J. Heeger, G.C. Bazan, Efficiency enhancement in low-bandgap polymer solar cells by processing with alkane dithiols, Nature Materials 6 (2007) 497–500.
[6] J. Hou, H.Y. Chen, S. Zhang, G. Li, Y. Yang, Synthesis, characterization, and photovoltaic properties of a low band gap polymer based on silole-containing polythiophenes and 2,1,3-benzothiadiazole, Journal of the American Chemical Society 130 (2008) 16144–16145.
[7] J. Hou, H.Y. Chen, S. Zhang, R.I. Chen, Y. Yang, Y. Wu, G. Li, Synthesis of a low band gap polymer and its application in highly efficient polymer solar cells, Journal of the American Chemical Society 131 (2009) 15586–15587.
[8] Y. He, G. Zhao, B. Peng, Y. Li, High-yield synthesis and electrochemical and photovoltaic properties of dndene-C_{70} bisadduct, Advanced Functional Materials 20 (2010) 3383–3389.
[9] Y. Sun, C. Cui, H. Wang, Y. Li, Efficiency enhancement of polymer solar cells based on poly(3-hexylthiophene)/indene-C_{70} bisadduct via methylthiophene additive, Advanced Energy Materials 1 (2011) 1058–1061.
[10] Y. Zhang, H.L. Yip, O. Acton, S.K. Hau, F. Huang, A.K.Y. Jen, A simple and effective way of achieving highly efficient and thermally stable bulk-heterojunction polymer solar cells using amorphous fullerene derivatives as electron acceptor, Chemistry of Materials 21 (2009) 2598–2600.
[11] R.F. Service, Outlook brightens for plastic solar cells, Science 332 (2011) 293.
[12] S.H. Park, A. Roy, S. Beaupré, S. Cho, N. Coates, J.S. Moon, D. Moses, M. Leclerc, K. Lee, A.J. Heeger, Bulk heterojunction solar cells with internal quantum efficiency approaching 100%, Nature Photonics 3 (2009) 297–302.
[13] Y. Liagn, Z. Xu, J. Xia, S.T. Tsai, Y. Wu, G. Li, C. Ray, L. Yu, For the bright future-bulk heterojunction polymer solar cells with power conversion efficiency of 7.4%, Advanced Materials 22 (2010) E135–138.
[14] T.Y. Chu, J. Lu, S. Beaupré, Y. Zhang, J.R. Pouliot, S. Wakim, J. Zhou, M. Leclerc, Z. Li, J. Ding, Y. Tao, Bulk heterojunction solar cells using thieno[3,4-c]pyrrole-4,6-dione and dithieno[3,2-b:2',3'-d]silole copolymer with a power conversion efficiency of 7.3%, Journal of the American Chemical Society 133 (2011) 4250–4253.
[15] J.K. Lee, W.L. Ma, C.J. Brabec, J. Yuen, J.S. Moon, J.Y. Kim, K. Lee, G.C. Bazan, A.J. Heeger, Processing additives for improved efficiency from bulk heterojunction solar cells, Journal of the American Chemical Society 130 (2008) 3619–3623.
[16] W.A Luhman, R.J. Holmes, Investigation of energy transfer in organic photovoltaic cells and impact on exciton diffusion length measurements, Advanced Functional Materials 21 (2011) 764–771.
[17] M.A. Ruderer, S. Guo, R. Meier, H.Y. Chiang, V. Körstgens, J. Wiedersich, J. Perlich, S.V. Roth, P. Müller-Buschbaum, Solvent-induced morphology in polymer-based systems for organic photovoltaics, Advanced Functional Materials 21 (2011) 3382–3391.
[18] W. Yin, M. Dadmun, A new model for the morphology of P3HT-PCBM organic photovoltaics from small-angle neutron scattering rivers and streams, ACS Nano 5 (2011) 4756–4768.
[19] D.H. Wang, J.S. Moon, J. Seifter, J. Jo, J.H. Park, O.O. Park, A.J. Heeger, Sequential processing: control of nanomorphology in bulk heterojunction solar cells, Nano Letters 11 (2011) 3163–3168.
[20] P.A. Staniec, A.J. Parnell, A.D.F. Dunbar, H. Yi, A.J. Pearson, T. Wang, P.E. Hopkinson, C. Kinane, R.M. Dalgliesh, A.M. Donald, A.J. Ryan, A. Iraqi, R.A.L Jones, D.G. Lidzey, The nanoscale morphology of a PCDTBT:PCBM photovoltaic blend, Advanced Energy Materirals 1 (2011) 499–504.
[21] B. Schmidt-Hansberg, M. Sanyal, M.F.G. Klein, M. Pfaff, N. Schnabel, S. Jaiser, A. Vorobiev, E. Müller, A. Colsmann, P. Scharfer, D. Gerthsen, U. Lemmer, E. Barrena, W. Schabel, Moving through the phase diagram: morphology

formation in solution cast polymer–fullerene blend films for organic solar cells, ACS Nano 5 (2011) 8579–8590.
[22] A.J. Moulé, K. Meerholz, Morphology control in solution-processed bulk-heterojunction solar cell mixtures, Advanced Functional Materials 19 (2009) 3028–3036.
[23] T. Wang, A.J. Pearson, D.G Lidzey, R.A.L. Jones, Evolution of structure, optoelectronic properties, and device performance of polythiophene:fullerene solar cells during thermal annealing, Advanced Functional Materials 21 (2011) 1383–1390.
[24] N.D. Treat, C.G. Shuttle, M.F. Toney, C.J. Hawker, M.L. Chabinyc, In situ measurement of power conversion efficiency and molecular ordering during thermal annealing in P3HT:PCBM bulk heterojunction solar cells, Journal of Materials Chemistry 21 (2011) 15224–15234.
[25] F. Padinger, R.S. Rittberger, N.S. Sariciftci, Effects of postproduction treatment on plastic solar cells, Advanced Functional Materials 13 (2003) 85–88.
[26] Y. Yao, J. Hou, Z. Xu, G. Li, Y. Yang, Effects of solvent mixtures on the nanoscale phase separation in polymer solar cells, Advanced Functional Materials 18 (2008) 1783–1789.
[27] B. Schmidt-Hansberg, M. Sanyal, N. Grossiord, Y. Galagan, M. Baunach, M.F.G. Klein, A. Colsmann, P. Scharfer, U. Lemmer, H. Dosch, J. Michels, E. Barrena, W. Schabel, Investigation of non-halogenated solvent mixtures for high throughput fabrication of polymer–fullerene solar cells, Solar Energy Materials and Solar Cells 96 (2012) 195–201.
[28] G. Li, Y. Yao, H. Yang, V. Shrotriya, G. Yang, Y. Yang, Solvent annealing effect in polymer solar cells based on poly(3-hexylthiophene) and methanofullerenes, Advanced Functional Materials 17 (2007) 1636–1644.
[29] G. Wei, S. Wang, K. Sun, M.E. Thompson, S.R. Forrest, Solvent-annealed crystalline squaraine: $PC_{70}BM$ (1:6) solar cells, Advanced Energy Materials 1 (2011) 184–187.
[30] H. Tang, G. Lu, L. Li, J. Li, Y. Wang, X. Yang, Precise construction of PCBM aggregates for polymer solar cells via multi-step controlled solvent vapor annealing, Journal of Materials Chemistry 20 (2010) 683–688.
[31] T.A. Bull, L.S.C. Pingree, S.A. Jenekhe, D.S. Ginger, C.K. Luscombe, The role of mesoscopic PCBM crystallites in solvent vapor annealed copolymer solar cells, ACS Nano 3 (2009) 627–636.
[32] S. Miller, G. Fanchini, Y.Y. Lin, C. Li, C.W. Chen, W.F. Su, M. Chhowalla, Investigation of nanoscale morphological changes in organic photovoltaics during solvent vapor annealing, Journal of Materials Chemistry 18 (2008) 306–312.
[33] F.C. Krebs, Fabrication and processing of polymer solar cells: a review of printing and coating techniques, Solar Energy Materials and Solar Cells 93 (2009) 394–412.
[34] K.X. Steirer, J.J. Berry, M.O. Reese, M.F.A.M. van Hest, A. Miedaner, M.W. Liberatore, R.T. Collins, D.S. Ginley, Ultrasonically sprayed and inkjet printed thin film electrodes for organic solar cells, Thin Solid Films 517 (2009) 2781–2786.
[35] G. Susanna, L. Salamandra, T.M. Brown, A. Di Carlo, F. Brunetti, A. Reale, Airbrush spray-coating of polymer bulk-heterojunction solar cells, Solar Energy Materials and Solar Cells 95 (2011) 1775–1778.
[36] A.J. Medford, M.R. Lilliedal, M. Jørgensen, D. Aarø, H. Pakalski, J. Fyenbo, F.C. Krebs, Grid-connected polymer solar panels: initial considerations of cost, lifetime, and practicality, Optical Express 18 (2010) A272–A285.
[37] F.C. Krebs, T. Tromholt, M. Jørgensen, Upscaling of polymer solar cell fabrication using full roll-to-roll processing, Nanoscale 2 (2010) 873–886.
[38] R. Søndergaard, M. Hösel, D. Angmo, T.T. Larsen-Olsen, F.C. Krebs, Roll-to-roll fabrication of polymer solar cells, Materials Today 5 (2012) 36–49.
[39] R.R. Søndergaard, M. Hösel, F.C. Krebs, Roll-to-roll fabrication of large area functional organic materials, Journal of Polymer Science Part B: Polymer Physics 51 (2013) 16–34.
[40] C. Girotto, D. Moia, B.P. Rand, P. Heremans, High-performance organic solar cells with spray-coated hole-transport and active layers, Advanced Functional Materials 21 (2011) 64–72.
[41] L.M. Chen, Z. Hong, W.L. Kwan, C.H. Lu, Y.F. Lai, B. Lei, C.P. Liu, Y. Yang, Multi-source/component spray coating for polymer solar cells, ACS Nano 4 (2010) 4744–4752.
[42] H.Y. Park, K. Kim, D.Y. Kim, S.K. Choi, S.M. Jo, S.Y. Jang, Facile external treatment for efficient nanoscale morphology control of polymer solar cells using a gas-assisted spray method, Journal of Materials Chemistry 21 (2011) 4457–4464.
[43] M.S. Kim, B.G. Kim, J. Kim, Effective variables to control the fill factor of organic photovoltaic cells, ACS Applied Materials and Interfaces 1 (2009) 1264–1269.
[44] Y.C. Huang, Y.C. Liao, S.S. Li, M.C. Wu, C.W. Chen, W.F. Su, Study of the effect of annealing process on the performance of P3HT/PCBM photovoltaic devices using scanning-probe microscopy, Solar Energy Materials and Solar Cells 93 (2009) 888–892.
[45] G. Li, V. Shrotriya, J. Huang, Y. Yao, T. Moriarty, K. Emery, Y. Yang, High-efficiency solution processable polymer photovoltaic cells by self-organization of polymer blends, Nature Materials 4 (2005) 864–888.
[46] M.Y. Chiu, U.S. Jeng, C.H. Su, K.S. Liang, K.H. Wei, Simultaneous use of small- and wide-angle X-ray techniques to analyze nanometerscale phase separation in polymer heterojunction solar cells, Advanced Materials 20 (2008) 2573–2578.